



Investigations on influencing the microstructure of additively manufactured Co-Cr alloys to improve subsequent machining conditions

Antonia Eissel¹ · Lorenz Engelking² · Kai Treutler¹ · Dirk Schroeppfer² · Volker Wesling¹ · Thomas Kannengiesser²

Received: 1 August 2022 / Accepted: 30 September 2022 / Published online: 12 October 2022
© The Author(s) 2022

Abstract

Co-Cr alloys are frequently used for highly stressed components, especially in turbine and plant construction, due to their high resistance to thermal and mechanical stress, as well as to corrosive and abrasive loads. Furthermore, they are classified as difficult-to-cut materials because of their high strength and toughness as well as their low thermal conductivity. However, for Co, an increased cost and supply risk can be observed in recent years. Therefore, additive manufacturing (AM) offers significant economic advantages due to higher material efficiency regarding repair, modification, and manufacturing of such components. Concerning inhomogeneity and anisotropy of the microstructure and properties as well as manufacturing-related stresses, a lot of knowledge is still necessary for the economic use of additive welding processes in SMEs. In addition, subsequent machining, particularly contour milling, is essential to generate the required complex contours and surfaces. Hence, additive and machining manufacturing processes need to be coordinated in a complementary way, especially due to additional challenges arising in milling of heterogeneous hard-to-cut microstructures. Recently, it has been shown that modern, hybrid cutting processes, such as ultrasonic-assisted milling (US), can improve the cutting situation. In this investigation, the Co-Cr initial alloy is additionally modified with Ti and Zr up to 1 wt% with the aim to enhance the homogeneity of the microstructure and, thus, the machinability. Hence the investigation includes finish milling tests of the AM components and the comparison of US and conventional machining. Both the modifications and the ultrasonic assistance exhibit a significant effect on the machining situation; for example US causes a higher surface integrity of the finish milled surfaces compared to conventional milling.

Keywords Cobalt-chromium alloy · Additive manufacturing · Ultrasonic-assisted milling · Surface integrity

1 Introduction

Components in today's turbine and plant engineering are increasingly exposed to a combination of corrosive, tribological and thermomechanical stresses. In such applications,

Co-Cr alloys are particularly predestined, due to their increased heat resistance combined with a high corrosion and wear resistance [1, 2]. Cr is the most important alloying element, as it acts as the principle carbide former and produces carbides mainly in the form of M_7C_3 , but also $M_{23}C_6$ [3–5]. This results in an increase in strength and enhances the oxidation and corrosion resistance of the alloy [6]. W and Mo also contribute to a higher strength [7]. At appropriate carbon content, these two elements form wear-resistant carbides and thus influence the morphology [8–10].

Considering the current developments in terms of emission reductions, as well as the increasing raw material prices of cobalt, there is a growing effort for energy, material and resource efficiency [11]. The key that fulfils these criteria, as well as the economic demand for lightweight construction and high deposition rates, is additive manufacturing (AM) and,

Recommended for publication by Commission IX - Behaviour of Metals Subjected to Welding

This article is part of the collection Additive Manufacturing Processes and Performance

✉ Antonia Eissel
antonia.eissel@tu-clausthal.de

Lorenz Engelking
lorenz.engelking@bam.de

¹ Institute of Welding and Machining (ISAF), Agricolastraße 2, 38678 Clausthal-Zellerfeld, Germany

² Federal Institute for Material Research and Testing (BAM), Unter den Eichen 87, 12205 Berlin, Germany

furthermore, the repair of such components using AM processes is of economic interest repair [12].

In addition, there are oftentimes further requirements for surface integrity under the specified loads, which is achieved by means of complementary additive and machining manufacturing steps. In general, due to the low thermal conductivity combined with high strength and toughness, Co-Cr alloys are challenging regarding economical machining with geometrically defined cutting edges [13]. A further factor is that as a rule additively manufactured components exhibit heterogeneous and anisotropic microstructures, which contributes to unstable cutting conditions and inconstant cutting forces during machining [14]. The microstructure has a direct effect on tool life, cutting forces and surface integrity. Some studies on different materials show positive effects on cutting forces and tool life associated with a finer microstructure [15–17]. For this reason, the interaction between metallurgy and machining is another important aspect to consider.

By using modern, hybrid machining processes it is possible to improve the machining situation. In the ultrasonic-assisted milling process (US), the kinematic of the conventional milling process (CM) is superimposed with an additional high-frequency oscillation in the micrometre range [18]. Schroepfer et al. performed finish milling experiments on AM specimens of IN725 and compared the USAM with the CM. They have found that US causes significantly lower cutting forces compared to CM [19]. Similar results were obtained in investigations of Rinck et al. on the influence of ultrasonic assistance on the machinability of Ti-6Al-4 V. Significantly reduced cutting forces due to US compared to CM were observed. In addition, for a small amplitudes of ultrasonic assistance of 4 μm , the US causes lower roughness values compared to the CM [18].

In the present work, the microstructure of a Co-Cr alloy is influenced by the addition of the monocarbide forming elements Ti and Zr [1], in order to achieve a homogeneous microstructure, implying positive influences on the subsequent machining process. Due to the focused setting of alloy modifications and the low degree of mixing, the investigations are based on plasma transferred-arc welding. In this context, the handling of powders for adjusting the modifications offers the particular advantage of influencing the microstructure and achieving more homogeneous and isotropic properties. The aim is to apply adequate AM welding process conditions to achieve a consistent and homogeneous microstructure that ensures stable situations for subsequent machining processes. Furthermore, the machinability depending on the alloy modification is studied and compared with a hybrid machining process (USAM) in addition to the conventional process (CM).

2 Material and methods

2.1 Materials used

The Co-Cr alloy being investigated is $\text{CoCr}_{26}\text{Ni}_9\text{Mo}_5\text{W}$. This Co-Cr alloy is characterized for its outstanding wear resistance even at high temperatures of 800 °C [2]. Furthermore, the alloy has a high corrosion resistance and is used in turbine and plant construction. The chemical composition is shown in Table 1.

For the different alloy modifications, Ti and Zr are added according to a statistical experimental design with a content of up to 1 wt% (see Table 2). Titanium is known as a fine grain former and causes a further increase in strength through precipitation hardening as a result of carbide and nitride formation [20]. Likewise, Zr is considered a strong carbide former [21]. Therefore, a positive effect of the elements on the microstructure morphology is expected depending on their concentration and/or combination. The powder modifications were realized by a 3D shaker mixer, which achieves a homogeneous mixture as a result of the rotatory, translatory movements and inversion.

2.1.1 Experimental setup

The welding experiments were performed with a PTA system. Argon 4.6+6.5% H_2 was used as shielding gas for the starting alloy and the modifications with zirconium only. These were welded with a base welding current of 130 A. Modifications with titanium were welded with pure Argon 4.6, as otherwise extreme pore formation would occur. Accordingly, a higher welding current of 220 A was required (see Table 2). The wall structures (approximately height \times length \times thickness = 50 \times 50 \times 20 mm^3) are each manufactured by multiple single-layer overlapping weld beads on low-alloy steel substrate (S355). In this process, the alloy systems are always applied one layer on each other in one direction and the necessary width is achieved by a pendulum

Table 1 Alloying elements $\text{CoCr}_{26}\text{Ni}_9\text{Mo}_5\text{W}$ in wt%

Alloy	Co	Cr	Ni	Mo	W	Fe	Mn	Si
$\text{CoCr}_{26}\text{Ni}_9\text{Mo}_5\text{W}$	Bal	26	9.2	5.3	1.9	3	0.8	0.5

Table 2 Design of experiments for alloy modifications

Experiment	Ti (%)	Zr (%)
1	1	0
2	0.33	0
3	0	1
4	0	0.33
5	1	1

motion. The interlayer temperature was 150 °C. All welding process influencing variables are listed in Table 3.

2.1.2 Metallurgical analysis and hardness measurements

A cross section was cut from the wall structure (or ingot) via wire EDM for specimen preparation. The cross section was divided into three parts and thus categorised into upper, middle and lower layers. For the light microscopic images, the specimens were embedded, ground and polished. The sample was etched with Beraha II for approximately 20 s to achieve a sufficiently high-contrast ratio of the micrographs [22]. Hardness analysis using HV 0.2 was performed centrally over the entire specimen cross section to investigate the properties of the microstructure in detail. Also HV10 hardness analysis was carried out for five individual measurements at varying locations on the cross section to identify the overall hardness of the alloy.

2.2 Machining experiments

The experimental setup of the finish-milling tests is shown in Fig. 1a. They were carried out in down milling

mode and under dry conditions on a 5-axis machining centre (DMU 65 by DMG MORI) modified for ultrasonic-assisted milling. The milling tool (by WOLF Werkzeugtechnik GmbH) used was a PVD-coated (TiAlSiN) solid carbide ball end milling cutter with four flutes and a diameter of 6 mm, which was tilted in the *x*- and in *y*-direction by 45° each. The specimens with dimensions of approximately 16 × 16 × 2 mm³ (length × width × height) were extracted from the AM ingots by electrical discharge machining (EDM) as shown in Fig. 1b. The specimens were machined perpendicular to the build direction. Tests with and without ultrasonic assistance (*P*_{US}) were carried out for each material, resulting in 12 milling experiments. The experimental data is shown in Table 4.

2.3 Cutting force analysis

The cutting forces occurring in the *x*- (feed force *F_f*), *y*- (feed normal force *F_{fN}*) and *z*-directions (passive force *F_p*) were analysed in situ using a multicomponent dynamometer (9139AA by KISTLER, time resolution: 0.1 ms). The resulting cutting force *F_{res}* was calculated according to Eq. (1):

Table 3 Welding process influencing variables

	Shielding gas	Welding current (A)	Welding voltage (V)	Welding speed (cm/min)	Width of pendulum (mm)	Intermediate-layer temperature (°C)
CoCr	Ar 4.6+6.5% H ₂	130	20	20	18	150
CoCr+0.33% Zr	Ar 4.6+6.5% H ₂	130	20	20	18	150
CoCr+1% Zr						
CoCr+0.33% Ti	Ar 4.6	130	20	20	18	150
CoCr+1% Ti						
CoCr+1% Ti+1% Zr	Ar 4.6	220	21	20	18	150

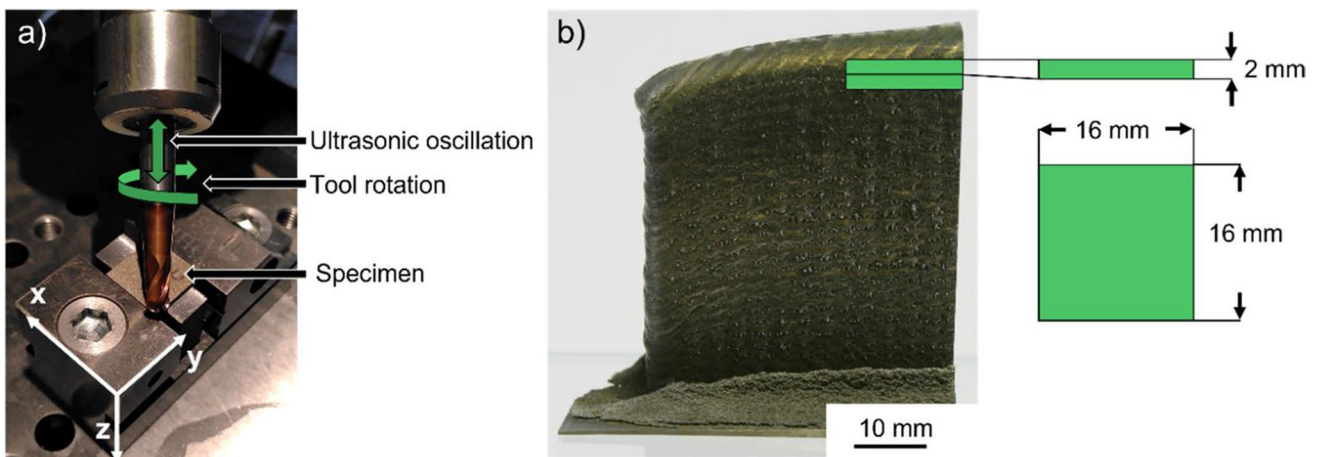


Fig. 1 a Experimental setup and (b) the exemplary sampling and the specimen dimensions

Table 4 Experimental data

Cutting speed $v_c = 70$ m/min	Feed rate $f_z = 0.055$ mm	Ultrasonic assistance $P_{US} = 0\%$ and 100%
Angle in x -direction $\lambda = 45^\circ$	Step over $a_e = 0.3$ mm	Ultrasonic frequency $F_{US} = 37.7 \pm 0.1$ kHz
Angle in y -direction $\tau = 45^\circ$	Cutting engagement $a_p = 0.3$ mm	Amplitude $A_{US} = 3 \mu\text{m} \pm 0.5 \mu\text{m}$

$$F_{\text{res}} = \sqrt{F_f^2 + F_{fN}^2 + F_p^2} \quad (1)$$

2.4 Roughness analysis

Roughness measurements were carried out using a light microscope (VHX-7000 by KEYENCE) with a measuring area of approximately 1 mm^2 according to DIN EN ISO 25178–3 standard [23] with a stitching image of five times five images at $1000\times$ magnification. Then, the average arithmetic height Sa , which is defined as the arithmetic mean of the absolute ordinate values within the defined range, was calculated [23]. For statistical certainty, the mean value was calculated from five measurements.

3 Results and discussion

3.1 Microstructure of $\text{CoCr}_{26}\text{Ni}_9\text{Mo}_5\text{W}$

The microstructure of the Co-Cr initial alloy is shown in Fig. 2. In the welded state, the alloy solidified with a dendritic microstructure. The microstructure consists of columnar Co-rich primary dendrites and regularly distributed secondary dendrites, as well as the interdendritic area (see Fig. 2). According to literature data, the interdendritic area are carbides of the M_7C_3 type [35]. The individual build-up layers can be clearly distinguished from each other due to the fan-shaped morphology at the contact zone. However, primary and secondary dendrites are still recognizable in the lower layer, whereas the primary dendrites in the upper layer grow away from the contact zone in a fan shape.

3.2 Microstructure of modifications

Microstructure investigation of the modifications with the alloying elements Ti and Zr (cf. Fig. 3) shows considerable effects on the microstructure. The number of secondary dendrite arms has been reduced in the modification with 1 wt% Ti compared to the initial alloy. The interdendritic phase contains fine titanium precipitates. Occasionally, interrupted columnar structure occurs, but predominantly a fine cluster-like distribution of the interdendritic phase

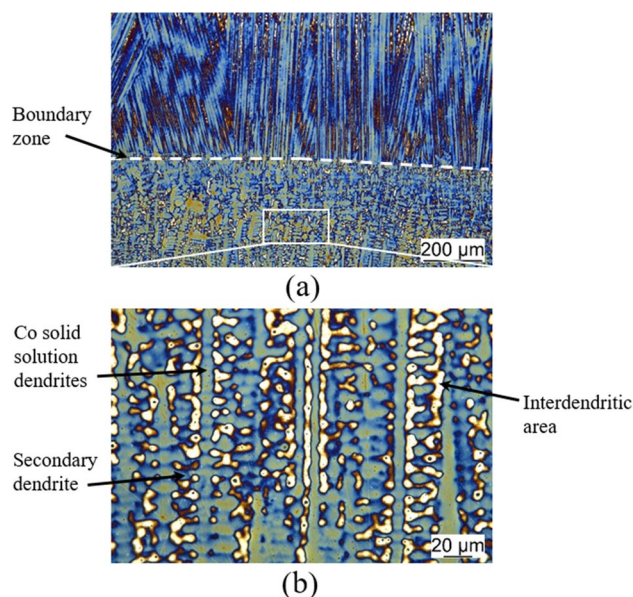


Fig. 2 Light microscopic images of microstructure of $\text{CoCr}_{26}\text{Ni}_9\text{Mo}_5\text{W}$ (a) and detail of dendritic microstructure (b) [24]

is formed. Lowering the content to 0.33 wt% Ti results also in less secondary dendrites and the microstructure consists mostly of columnar primary dendrites. The length of the interdendritic domains has increased compared to 1 wt% Ti and has become largely columnar throughout. The homogeneity of these modified microstructures is significantly enhanced.

In comparison to the modification with 1 wt% Ti, the number of secondary dendrites is again significantly reduced in the modification with 1 wt% Zr. In addition, the interdendritic areas are disrupted, significantly shortened in length, and regularly finely distributed in the microstructure. The precipitates caused by Zr form crescentic or rhombic shapes in both the Co solid solution and the interdendritic regions. A reduction of Zr to 0.33 wt% also shows a homogeneous microstructure. The number of secondary dendrites is also increased and a mesh-like structure appears. Therefore, the Zr precipitates form only cubic and rhombic shapes and are primarily enclosed by the interdendritic areas.

The microstructure in the depth direction of the initial alloy is also compared with the modification with 1 wt% Zr (see Fig. 4). It can be seen that with the addition of zirconium, a more homogeneous and uniform distribution of the interdendritic area stiffness can be observed as well.

The combination of 1 wt% Ti and 1 wt% Zr significantly narrows the interdendritic regions and forms primarily around the precipitates. The number of secondary dendrite arms is the lowest compared to the other modifications and the initial alloy. However, some large cracks with an average length of $5.8 \mu\text{m}$ have formed in the centre of the cross section in the ingot of this alloy (see Fig. 5).

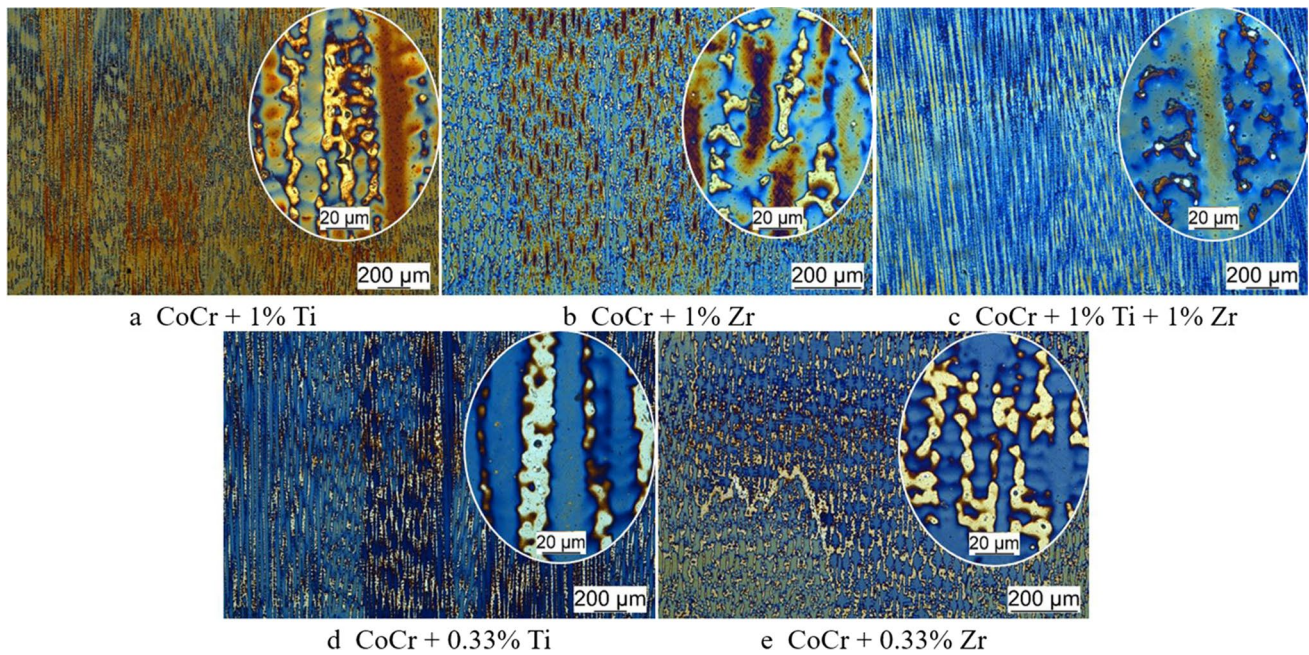
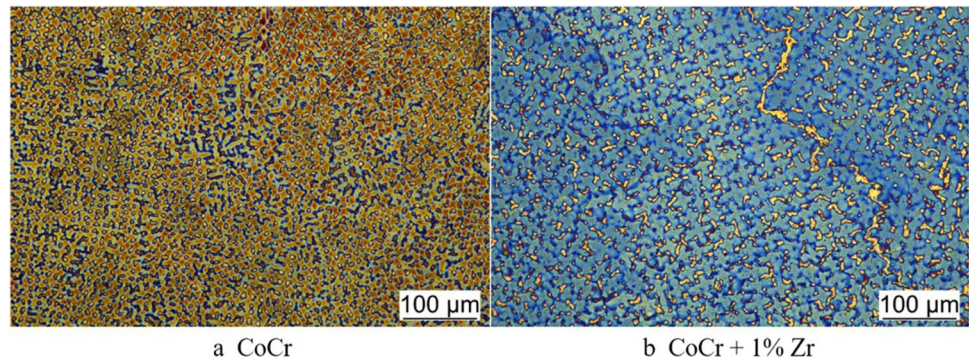


Fig. 3 Light microscopic images of the microstructure of **a** $\text{CoCr}_{26}\text{Ni}_9\text{Mo}_5\text{W} + 1\% \text{Ti}$, **b** $\text{CoCr}_{26}\text{Ni}_9\text{Mo}_5\text{W} + 1\% \text{Zr}$, **c** $\text{CoCr}_{26}\text{Ni}_9\text{Mo}_5\text{W} + 1\% \text{Ti} + 1\% \text{Zr}$, **d** $\text{CoCr}_{26}\text{Ni}_9\text{Mo}_5\text{W} + 0.33\% \text{Ti}$, and **e** $\text{CoCr}_{26}\text{Ni}_9\text{Mo}_5\text{W} + 0.33\% \text{Zr}$ (partly shown in [24])

Fig. 4 Light microscopic images of the microstructure in depth direction of **a** $\text{CoCr}_{26}\text{Ni}_9\text{Mo}_5\text{W}$ and **b** $\text{CoCr}_{26}\text{Ni}_9\text{Mo}_5\text{W} + 1\% \text{Zr}$



3.3 Hardness measurements

For a detailed analysis of the microstructure components, the hardness with HV 0.2 is analysed centred over the cross section of the entire specimen (cf. Fig. 5). A large scatter is obvious, which is because of the hardness gradients between the Co matrix and the harder interdendritic region. As a result of this scatter, the values are also shown using mathematical smoothing filter, which is indicated by a dashed line in Fig. 6. Position zero marks the top layer and with increasing position value the middle and lower layers are measured. The length of the curves varies depending on the height of the wall structure. The hardness values of the initial alloy and the modifications are between 260 HV 0.2 and 340 HV 0.2.

The hardness of the initial alloy is lower in the upper layers compared to the lower layers. One reason is that in the

lower layers there is still a lot of mixing with the substrate plate. Likewise, the upper layers do not experience recurrent heating compared to the middle and lower layers. The different hardness profiles of Ti modifications are caused by microstructure morphology. The hardness profile of 0.33 wt% Ti is quantitatively higher than 1 wt% Ti due to a more homogeneous distribution of the interdendritic phase. The hardness profile of the modifications with 1 wt% Zr is lower than profiles of other modifications and the initial alloy, since the interdendritic region is finely dispersed. Based on its mesh-like morphology, the modification with 0.33 wt% Zr exhibits higher hardness profile compared to all other alloys. The modification with 1 wt% Ti + 1 wt% Zr shows a hardness level around 300 HV 0.2.

The five individual hardness measurements with HV 10 of the upper and middle layers are shown in Fig. 7.

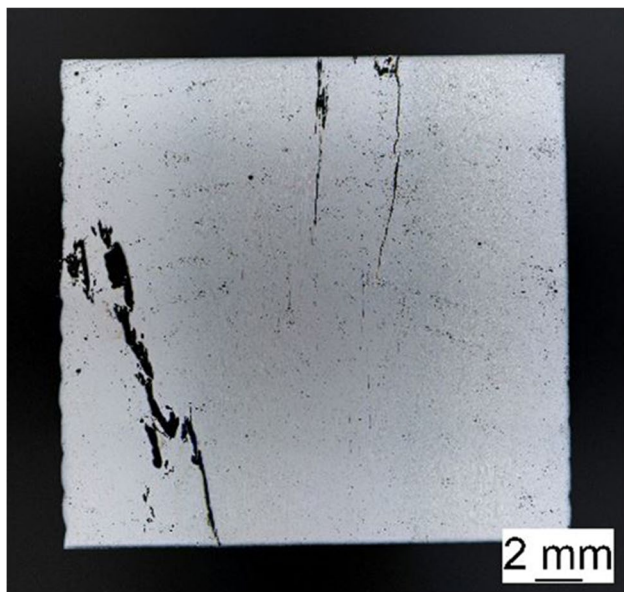
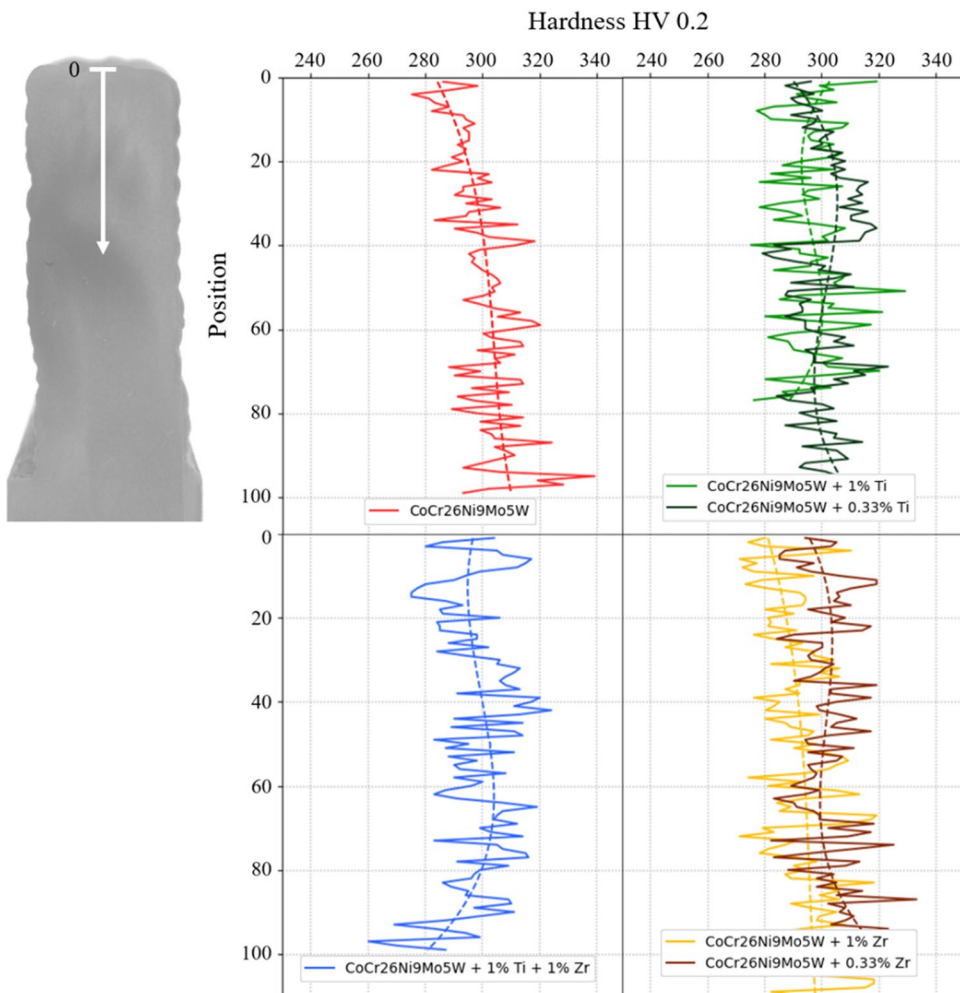


Fig. 5 Occurring cracks exemplified by the middle layers of $\text{CoCr}_{26}\text{Ni}_9\text{Mo}_5\text{W} + 1\% \text{Ti} + 1\% \text{Zr}$

Fig. 6 Hardness measurement series HV 0.2 over the entire cross section



The arithmetic mean values over the measurements were determined (black square). For the upper layers, the averaged hardness increases slightly for each modification compared to the initial alloy. The modification $\text{CoCr} + 1 \text{ wt}\% \text{Ti} + 1 \text{ wt}\% \text{Zr}$ shows a larger scatter than the other modifications, indicating imperfections. In addition, the hardness in the depth direction was measured for the initial alloy and exemplary the modification 1 wt% Zr. These differ only minimally from the equivalent average hardness of the cross section. Thus, the starting alloy has an average hardness of 278 HV 10. The average hardness of 1 wt% Zr is slightly below the cross section at 255 HV 10.

3.4 Machining analyses

3.4.1 Cutting force

Figure 8a shows the three in-situ analysed cutting force components feed force F_f , feed normal force F_{fN} , passive force F_p and the calculated resulting cutting force F_{res} exemplarily for one milling line and in Fig. 8b for one tool rotation. One peak corresponds to one cutting engagement each.

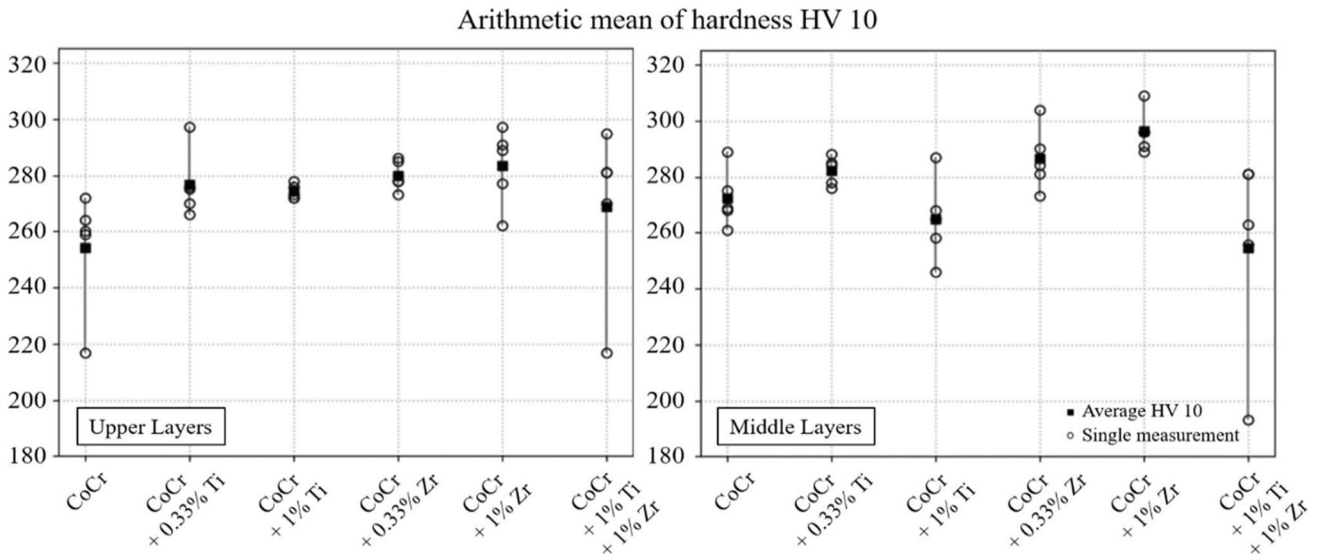


Fig. 7 Hardness measurement HV 10 of Co-Cr initial alloy and the modifications — upper layers (left) and middle layers (right)

Figure 9a shows the resulting cutting force F_{res} as a function of the alloy modification for CM (Fig. 9b for US). The statistical evaluation exhibits no significant effect of ultrasonic assistance in this respect, as both processes show more or less similar contour plots (cf. Fig. 9a and b). The modification with 1 wt% Zr indicates the lowest resulting cutting force compared to the Co-Cr initial alloy, which is the case for both machining processes. It is assumed that this is due to the microstructure alteration, i.e. its fine distributed and decreased interdendritic areas compared to the microstructure of the Co-Cr initial alloy (cf. Section 3.2). For lower modification content of 0.33 wt% Zr, a slight increase in the

resulting cutting force compared to the Co-Cr initial alloy can be observed for both processes. This effect may be the result of the increase of the interdendritic regions compared to the modification with 1 wt% Zr (cf. Section 3.2). Ti significantly affects the resulting cutting force, which could be traced back on the hard Ti precipitates in these alloy modifications (cf. Section 3.2). The precipitates formed by Ti have a higher influence on the resulting cutting force compared to the precipitates formed by Zr. The addition of 0.33 wt% Ti to the Co-Cr initial alloy results in a significant increase in the resulting cutting force for both processes (cf. Fig. 3a and b), which is further increased for the modification with 1 wt%

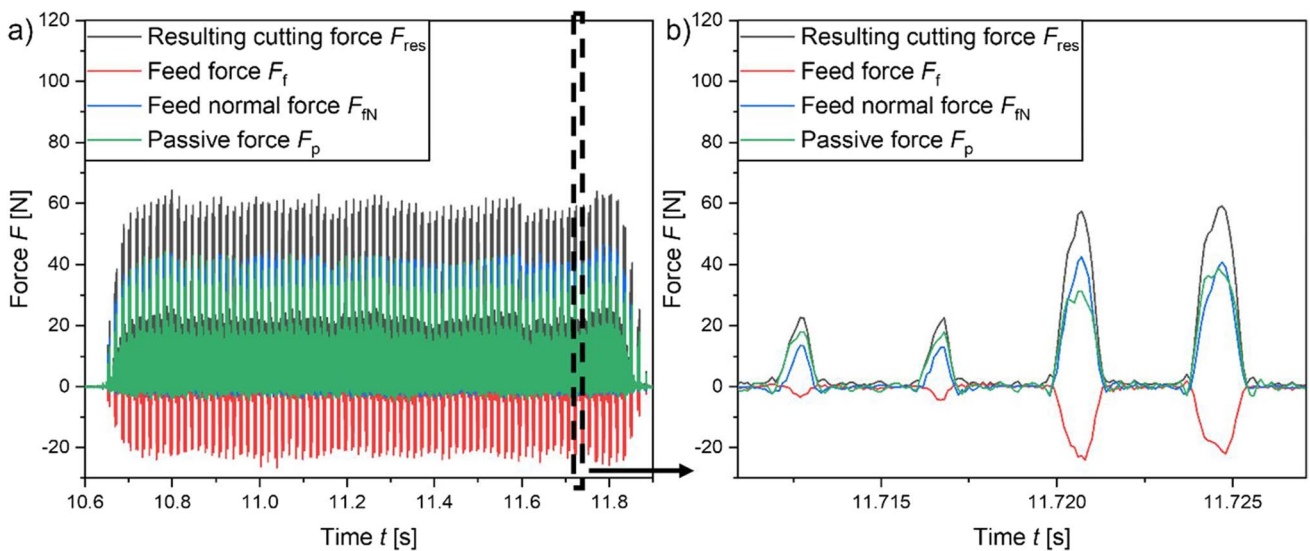
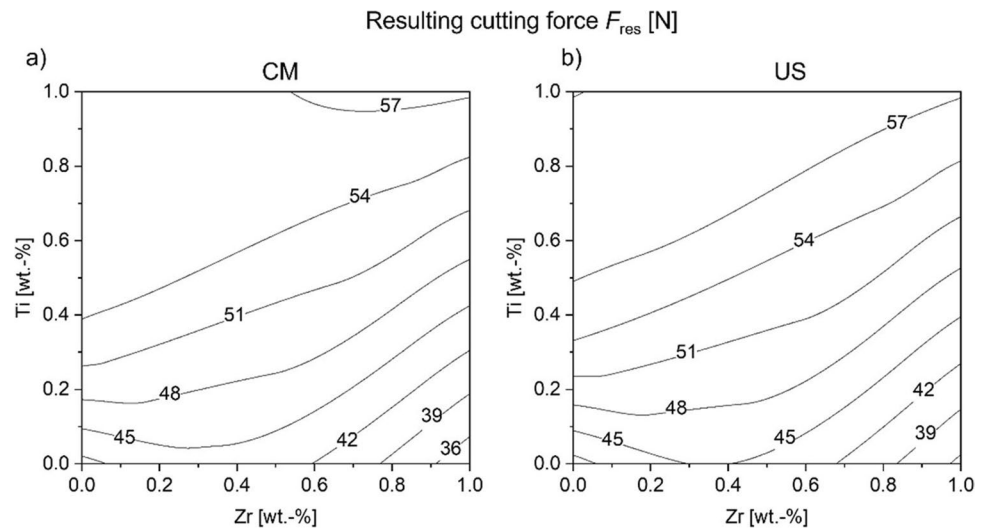


Fig. 8 Exemplary representation of the cutting forces F_f , F_{fn} and F_p as well as the resulting cutting force F_{res} during milling: (a) one milling line and (b) one tool revolution of CM of CoCr+0.33 wt% Zr

Fig. 9 Contour plots of resulting cutting force F_{res} vs. alloy modification of Zr and Ti for (a) CM and (b) US



Ti. Ti alloy modification lead to somewhat higher resulting cutting force for US compared to CM. Combined modification with 1 wt% Zr + 1 wt% Ti causes a significant increase in the resulting cutting force for both processes compared to the Co-Cr initial alloy for both milling processes. It is assumed that although the interdendritic regions of this modification are the smallest of all materials investigated, the precipitates within these interdendritic areas are capable to lead to considerable cutting force increase (cf. Section 3.2).

3.5 Roughness

Figure 10 shows the average arithmetic height S_a as a function of the material. Note that only those alloy modifications were examined in which no cracks occurred (cf. Section 3.2). The modification with 0.33 wt% Zr shows a trend of reduced roughness for

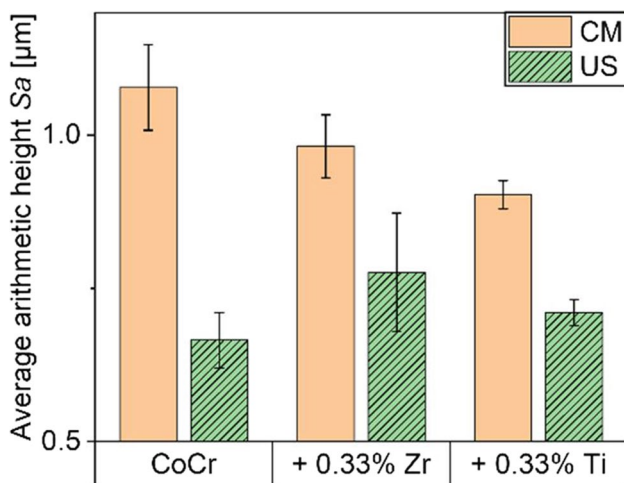


Fig. 10 Average arithmetic height S_a vs. alloy modification for US and CM process

the CM compared to the Co-Cr initial alloy, which is however not significant. The addition of 0.33 wt% Ti to the Co-Cr initial alloy results in a significant reduction of roughness for the CM compared to the Co-Cr initial alloy. It is assumed that the more homogeneous microstructure of the modification with 0.33 wt% Ti compared to the Co-Cr initial alloy and an associated more stable machining process is responsible for the reduced roughness. The US process significantly reduces the roughness for all three materials investigated, also observed by other authors. They attributed this effect to a decreased amount of feed marks on the surface of the US milled specimens compared to the surfaces generated by CM [18]. The roughness values for US are approximately in the same range for all three materials.

4 Conclusion

Modifying the Co-Cr alloy with different contents of Ti and Zr up to 1 wt% shows significant effects on the welded solidification morphology, as well as the subsequent machinability.

- (1) Zr reduces the interdendritic phases and become finely homogeneously distributed in the microstructure, particularly pronounced at 1 wt% Zr.
- (2) Modification of 1 wt% Zr to the Co-Cr alloy reduces resulting cutting forces during milling.
- (3) The precipitates formed by Ti also reduce the interdendritic phase. The lower content of 0.33 wt% Ti leads to a homogeneous microstructure as well.
- (4) Ti modifications significantly increase the resulting cutting force in the performed milling tests.
- (5) The roughness of the milled surface for CM of 0.33 wt% Ti-modified specimens is decreased compared to the initial Co-Cr alloy.

- (6) The combined modification of 1 wt% Ti and 1 wt% Zr shows a highly directional microstructure with significant reduction of the interdendritic areas.
- (7) The ultrasonic assistance P_{US} shows significantly beneficial effects on lower roughness values for all materials investigated.

Acknowledgements We would like to thank for this funding and the companies and persons involved in the project committee for the support, in particular WOLF Werkzeugtechnologie GmbH for providing the milling tools. We also thank Sabine Friederichs from ISAF for her support in the preparation of the microstructure and the hardness measurements, Andreas Boerner from BAM for his support in the milling experiments and Sephrdad Dorrani for his support in the cutting force and roughness analysis.

Funding Open Access funding enabled and organized by Projekt DEAL. The IGF project IGF No. 20.979 N (DVS 01.3211) of the Research Association of the DVS was supported by the Federal Ministry for Economic Affairs and Climate Action by the AiF as part of the program for support of the cooperative industrial research (IGF) on the basis of a decision by the German Bundestag.

Declarations

Conflict of interest The authors declare no competing interests.

Open Access This article is licensed under a Creative Commons Attribution 4.0 International License, which permits use, sharing, adaptation, distribution and reproduction in any medium or format, as long as you give appropriate credit to the original author(s) and the source, provide a link to the Creative Commons licence, and indicate if changes were made. The images or other third party material in this article are included in the article's Creative Commons licence, unless indicated otherwise in a credit line to the material. If material is not included in the article's Creative Commons licence and your intended use is not permitted by statutory regulation or exceeds the permitted use, you will need to obtain permission directly from the copyright holder. To view a copy of this licence, visit <http://creativecommons.org/licenses/by/4.0/>.

References

1. Sims CT, Stoloff N, Hage W (1987) Superalloys II - High-Temperature Materials for Aerospace and Industrial Power. New York: Wiley
2. Berns H, Fischer A (1993) Tribological stability of metallic materials at elevated temperatures. *Wear* 162–164:441–449
3. Frenk A, Kurz W (1994) Microstructural effects on the sliding wear resistance of a cobalt-based alloy. *Wear* 174(1–2):81–91
4. Park JB, Jung K-H, Kim KM, Son Y, Lee J-I, Ryu JH (2018) Microstructure of as-cast Co-Cr-Mo alloy prepared by investment casting. *J Korean Phys Soc* 72(8):947–951
5. Zangeneh S, Farhangi H (2010) Influence of service-induced microstructural changes on the failure of a cobalt-based superalloy first stage nozzle. *Mater Design* 31(7):3504–3511
6. Bettini E, Eriksson T, Boström M, Leygraf C, Pan J (2011) Influence of metal carbides on dissolution behavior of biomedical CoCrMo alloy: SEM, TEM and AFM studies. *Electrochimica Acta* 56(25):9413–9419
7. Liu R, Xi SQ, Kapoor S, Wu XJ (2010) Effects of chemical composition on solidification, microstructure and hardness of Co-Cr-W-Ni and Co-Cr-Mo-Ni alloy systems. *Int J Res Rev Appl Sci* 5(2):110–122
8. Davis JR (2000) Nickel, cobalt, and their alloys. ASM specialty handbook. Materials Park, Ohio: ASM International
9. Giacchi JV, Morando CN, Fornaro O, Palacio HA (2011) Microstructural characterization of as-cast biocompatible Co–Cr–Mo alloys. *Mater Charact* 62(1):53–61
10. Lin Z, Ya W, Subramanian VV, Goulas C, Di Castri B, Hermans MJM, Pathiraj B (2020) Deposition of Stellite 6 alloy on steel substrates using wire and arc additive manufacturing. *Int J Adv Manuf Technol* 111(1–2):411–426
11. Hertwich E, Lifset R, Pauliuk S, Heeren N (2021) United Nations Environment Programme - Resource Efficiency and Climate Change. Material efficiency strategies for a low-carbon future. UNESCO, <https://doi.org/10.5281/zenodo.3542680>
12. Frazier WE (2014) Metal additive manufacturing: a review. *J Mater Eng Perform* 23(6):1917–1928
13. Shokrani A, Dhokia V, Newman ST (2012) Environmentally conscious machining of difficult-to-machine materials with regard to cutting fluids. *Int J Mach Tools Manuf* 57:83–101
14. Alexander I, Vladimir G, Petr P, Mihail K, Yuriy I, Andrey V (2016) Machining of thin-walled parts produced by additive manufacturing technologies. *Procedia CIRP* 41:1023–1026
15. Pan Z, Feng Y, Liang SY (2017) Material microstructure affected machining: a review. *Manufacturing Rev* 4(5). <https://doi.org/10.1051/mfreview/2017004>
16. Dang J, Cai X, Yu D, An Q, Ming W, Chen M (2019) Effect of material microstructure on tool wear behavior during machining additively manufactured Ti6Al4V. *Arch Civil Mech Eng* 20. <https://doi.org/10.1007/s43452-019-0007-7>
17. Denkena B, Grove T (2016) The effect of microstructure on the machinability of Ti-6Al-4V. *Proceedings of the 13th World Conference on Titanium*, 905–910. <https://doi.org/10.1002/9781119296126.ch155>
18. Rinck PM, Gueray A, Kleinwort RU, Zaeh MF (2020) Experimental investigations on longitudinal-torsional vibration-assisted milling of Ti-6Al-4V. *Int J Adv Manuf Technol* 108(11–12):3607–3618
19. Schroepper D, Treutler K, Boerner A, Gustus R, Kannengiesser T, Wesling VU, Maus-Friedrichs W (2021) Surface finishing of hard-to-machine cladding alloys for highly stressed components. *Int J Adv Manuf Technol* 114(5–6):1427–1442
20. Dilthey U (2005) *Schweißtechnische Fertigungsverfahren 2 - Verhalten der Werkstoffe beim Schweißen*. Springer: Berlin
21. Arnold B (2019) *Zirkon, Zirkonium, Zirkonia - ähnliche Namen, verschiedene Materialien*. Springer: Berlin, <https://doi.org/10.1007/978-3-662-59579-4>
22. Weck E, Leistner E (1983) Metallographic instruction for colour etching by immersion: colour etching of low-alloy and high-alloy steels nickel-based alloys and cobalt-based alloys Pt. 2. *Fachbuchreihe Schweißtechnik*, Bd. 77. DVS Media GmbH: Düsseldorf
23. DIN EN ISO 25178-2:2020-02 (2020) Geometrical product specifications (GPS) - Surface texture: Areal - Part 2: Terms, definitions and surface texture parameters (ISO/DIS 25178-2:2019)
24. Eissel A, Engelking L, Treutler K, Schröpfer D, Wesling V, Kannengießner T (2022) Modification of Co–Cr alloys to optimize additively welded microstructures and subsequent surface finishing. *Welding in the World* 66: 2245–2257. <https://doi.org/10.1007/s40194-022-01334-0>

Publisher's note Springer Nature remains neutral with regard to jurisdictional claims in published maps and institutional affiliations.